PERGAMON

International Journal of Solids and Structures 38 (2001) 335–351

INTERNATIONAL JOURNAL OF SOLIDS and STRUCTURES

www.elsevier.com/locate/ijsolstr

Use of scaling functions to determine mechanical properties of thin coatings from microindentation tests

Karuna Tunvisut, Noel P. O'Dowd *, Esteban P. Busso

Department of Mechanical Engineering, Imperial College of Science, Technology and Medicine, London SW7 2BX, UK

Received 26 May 1999; in revised form 16 December 1999

Abstract

The indentation of elastic–plastic coatings deposited on elastic substrates is studied in this work. The functional expressions that relate the load–indentation behaviour to coating and substrate material properties are derived using dimensional analysis in conjunction with finite element simulations. Based on these scaling functions, a method is proposed to determine the coating Young's modulus, yield strength and strain hardening properties from the micro-indentation tests. A method to obtain improved estimates of the material hardness is also discussed. While the analyses are based on a conical (i.e. Rockwell) indenter, the indenter angle used in the simulations was selected so that the results can also be used to extract mechanical properties from measurements using the pyramidal indenters such as Vickers and Berkovich types.

Keywords: Indentation; Mechanical properties of coating; Finite element simulation

1. Introduction

Indentation techniques have been used extensively to determine directly the material hardness or, indirectly, the bulk mechanical properties when other methods have proven to be unsuitable. In particular, as indentation techniques have improved, micro-indentation has become the most popular method for studying the mechanical properties of thin films and coatings (Pharr et al., 1995; Vlassak et al., 1999a,b) where, due to the microstructural differences, the in situ properties of the coating may differ considerably from the nominal, bulk properties.

A number of methods based on experimental and numerical studies have been proposed to extract mechanical properties from indentation load–displacement curves on the uncoated substrates, e.g. Doerner and Nix (1986), Oliver and Pharr (1992), Cheng and Cheng (1999). For example, Young's modulus and yield strength can be calculated approximately from the peak load and the initial slope of the unloading curves using the method of Oliver and Pharr (1992) or that of Cheng and Cheng (1999). Finite element techniques have been used more directly to extract the mechanical properties of materials by matching the

* Corresponding author. Tel.: +44-171-594-7059; fax: +44-171-823-8845.
E-mail address: n.odowd@ic.ac.uk (N.P. O'Dowd).

0020-7683/00/$ - see front matter
PII: S0020-7683(00)00017-2

simulated loading and unloading curves with the experimental ones (Bhattacharya and Nix, 1988; Laursen and Simo, 1992; Knapp et al., 1999).

Simple theoretical solutions have also been developed to interpret the indentation curves involving uncoated substrates. In one of the earliest studies by Sneddon (1965), the load–displacement relationship for the indentation of an elastic substrate with a conical (Rockwell type) indenter was given as

$$F = \alpha h^2, \tag{1}$$

where F is the indentation load, h, the indentation depth, and α, a constant depending on the substrate elastic properties. In practice, this equation is relevant only for materials in which the ratio of the elastic modulus to the yield stress is very low (Sneddon, 1965). The so-called cavity model (Johnson, 1985) has been developed to predict the load–indentation curve of an elastic, perfectly plastic material using a conical indenter. The model assumes that the contact surface of the indenter is encased in a hemispherical 'core'. Within the core, a constant hydrostatic component of stress, $\overline{p}$ is assumed. Outside the core, the stresses and displacements have a radial symmetry and are the same as in an infinite elastic, perfectly plastic body which contains a spherical cavity under a pressure $\overline{p}$. The pressure $\overline{p}$ is then given by

$$\overline{p} = \frac{2}{3}\sigma_y\left\{1 + \ln\left(\frac{1}{3}\frac{E\cot\theta}{\sigma_y}\right)\right\}, \tag{2}$$

where σ_y is the material yield strength, E the Young's modulus, and θ, the cone half-angle (Fig. 1). The indentation pressure p (i.e. σ_z) is then

$$p = \overline{p} + \frac{2}{3}\sigma_y, \tag{3}$$

which, when multiplied by the projected indentation area, gives an estimate of the indentation load,

$$F = \frac{2\sigma_y}{3}\pi(h\tan\theta)^2\left\{2 + \ln\left(\frac{1}{3}\frac{E\cot\theta}{\sigma_y}\right)\right\}. \tag{4}$$

It can be seen that the parabolic relationship between load, F, and indentation depth, h, found in the elastic case (Eq. (1)), is preserved in this model.

No such simple analytical or semi-analytical solutions are currently available for the indentation of a coated system. In this work, relationships for a conical indentation are developed using dimensional analysis in conjunction with a finite element-based parametric studies of coated systems. A new method-

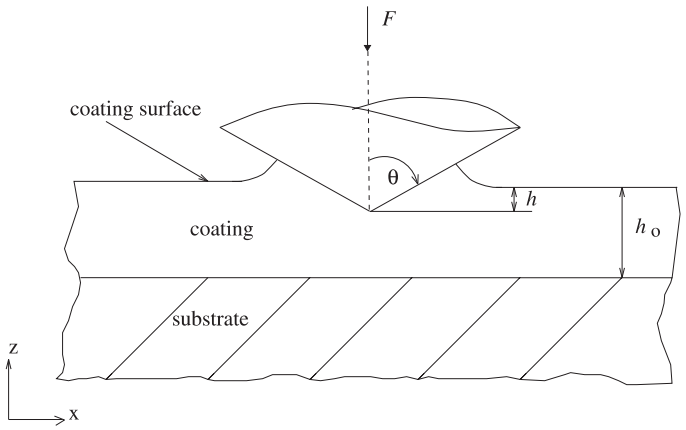

Fig. 1. An illustration of the conical indenter.

ology for the determination of the elastic–plastic material properties of the coating is also proposed. Although the results presented here are based on the analysis of a conical indenter, it will be shown that they are also applicable to the analysis of indentation curves produced by indenters of the Vickers and Berkovich types. This work extends the analysis of Cheng and Cheng (1998a,b,c, 1999) where similar relations were derived for the *uncoated* substrates.

2. Dimensional analysis of the indentation of a coated substrate

Consider the rigid, conical indenter with a half angle θ, indenting into an elastic–plastic coating shown in Fig. 1, characterised by a Young's modulus (E_c), yield strength (σ_{yc}), Poisson's ratio (ν_c) and strain hardening exponent (n_c). The tensile behaviour of coating is described by a power law relation, viz.,

$$\tilde{\epsilon}/\epsilon_y = (\tilde{\sigma}/\sigma_y)^n, \tag{5}$$

where $\tilde{\epsilon}$ and $\tilde{\sigma}$, are the von Mises strain and stress, respectively, ϵ_y, the yield strain of the material ($= \sigma_y/E$), and n, the strain hardening exponent. The substrate material is, in turn, assumed to be a linear elastic, characterised by a Young's modulus (E_s) and Poisson's ratio (ν_s). Thus, it is implicitly assumed that the substrate yield strength is much higher than that of the coating material. It is also assumed that there is no friction between the indenter and the coating surface, i.e., the coating and indenter are both considered to be microscopically smooth.

A typical load–indentation curve is illustrated in Fig. 2, identifying the loading and unloading portions of the curve. The maximum indentation depth, h_m, the corresponding maximum load, F_{max}, and the indentation depth after unloading, h_f, are also shown. In what follows, dimensionless relationships to describe the indentation behaviour of the coated substrates for a wide range of material combinations are derived. The loading part of the curve is first examined and relevant dimensionless relationships are extracted; the unloading behaviour is then analysed.

During loading, the magnitude of the indentation force (F), depends on the elastic–plastic properties of the coating/substrate materials (E_c, σ_{yc}, ν_c, n_c, E_s, ν_s), the coating thickness (h_o), the indentation depth (h), and the indenter half angle (θ):

$$F = \hat{F}_L(E_c, \sigma_{yc}, \nu_c, n_c, E_s, \nu_s, h, h_o, \theta). \tag{6}$$

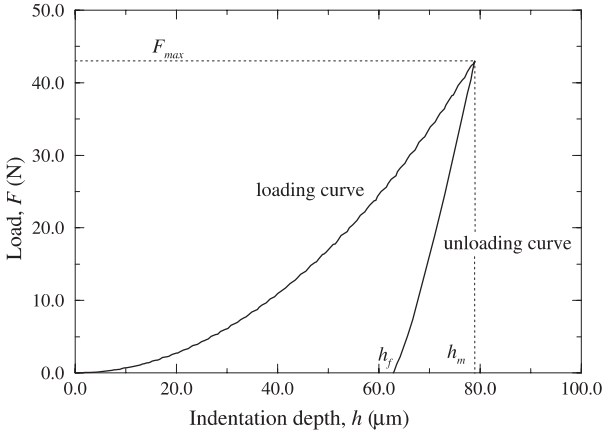

Fig. 2. A typical indentation curve for a ductile material.

In this work, it is assumed that the properties of the substrate (E_s, ν_s) and the coating thickness h_o are known and the goal is to determine the coating properties (E_c, σ_{yc}, ν_c, n_c). By applying the Buckingham PI theorem (Barenblatt, 1996) and choosing the normalisation so that unknown quantities are normalised by known quantities, the following dimensionless relationship can be obtained:

$$\frac{F}{h_o^2 E_s} = \hat{\Pi}_\alpha\left(\frac{h}{h_o}, \frac{E_c}{E_s}, \frac{\sigma_{yc}}{E_s}, \nu_c, \nu_s, n_c, \theta\right). \tag{7}$$

Once the maximum indentation depth (h_m) is reached, and the load is removed, the unloading force F then exhibits an additional dependence on h_m. Thus, Eq. (6) becomes

$$F = \hat{F}_U(E_c, \sigma_{yc}, \nu_c, n_c, E_s, \nu_s, h, h_o, \theta, h_m). \tag{8}$$

Dimensional analysis of the above gives

$$\frac{F}{h_o^2 E_s} = \hat{\Pi}_\beta\left(\frac{h}{h_o}, \frac{h_m}{h_o}, \frac{E_c}{E_s}, \frac{\sigma_{yc}}{E_s}, \nu_c, \nu_s, n_c, \theta\right). \tag{9}$$

Note that the unloading slope of the indentation curve is not constant due to the large geometry changes on unloading, see Fig. 2. Then, if one considers the initial slope dF/dh at the onset of unloading, the following relationship is obtained:

$$\frac{1}{h_o E_s}\left.\frac{dF}{dh}\right|_{h=h_m} = \hat{\Pi}_\delta\left(\frac{h_m}{h_o}, \frac{E_c}{E_s}, \frac{\sigma_{yc}}{E_s}, \nu_c, \nu_s, n_c, \theta\right), \tag{10}$$

where $\hat{\Pi}_\delta$ represents the first derivative of $\hat{\Pi}_\beta$ in Eq. (9) with respect to h/h_o. As it is not possible to determine the function $\hat{\Pi}_\beta$ in Eq. (9) analytically, this differentiation cannot be carried out directly. Instead, $\hat{\Pi}_\delta$ will be calibrated numerically from the finite element calculations.

Having obtained the functional dependence of these dimensionless scaling functions, $\hat{\Pi}_\beta$, $\hat{\Pi}_\delta$, numerical analyses can be performed to quantify the functional relationships given by Eqs. (7) and (10). The numerical procedures used to carry out the analyses are next discussed and solutions for the functions $\hat{\Pi}_\beta$ and $\hat{\Pi}_\delta$ over the range of interest are presented.

3. Finite element model

The coated system was modelled as a cylinder with a thin coating on its surface, (Fig. 3). The indenter angle chosen in the analysis was $\theta = 70°$. A very fine mesh was used in the contact region to ensure a high degree of numerical accuracy, and a gradually coarser mesh was employed both at the surface and in the interior of the specimen. Mesh resolution studies were carried out in order to obtain a convergent solution, and the final mesh used in the analysis contained 2500 four-noded axisymmetric elements. For the coated substrates, 48 elements were used through the coating thickness. The loading and unloading curves were obtained directly from the finite element output of the normal reaction force on the rigid indenter, as a function of the vertical displacement of the node directly beneath the tip of the indenter. The finite element code ABAQUS (1996) was used in all the simulations.

4. On the use of a conical indenter

The assumption of a conical indenter allowed the problem to be modelled using two-dimensional axisymmetric elements. The chosen angle of 70° gives the same area-to-depth ratio as the Berkovich three-

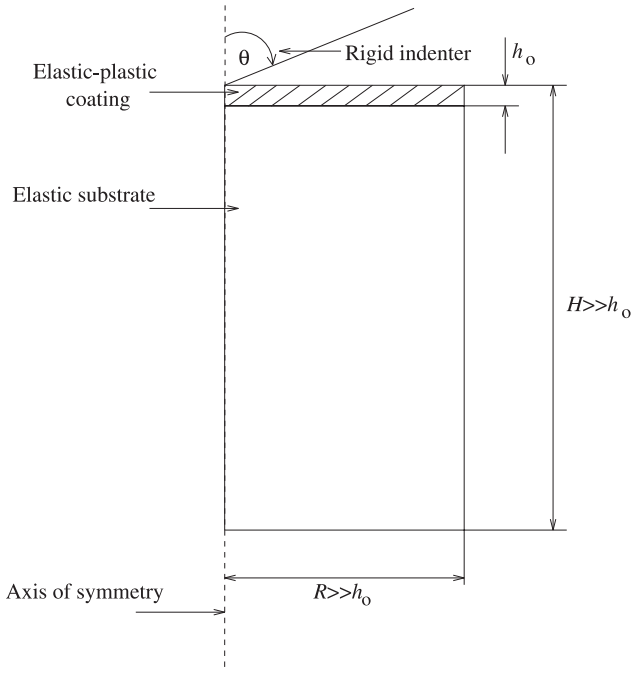

Fig. 3. Geometry of the indentation problem (not to scale).

sided pyramid and Vickers four-sided pyramid indenters used in micro-hardness testing (Bolshakov and Pharr, 1998). In the previous work (Cheng and Cheng, 1998a,b,c), a good agreement was obtained between the experimental Berkovich indentation curves and finite element predictions. To confirm the applicability of the 70° conical indenter in predicting Vickers indentation curves, finite element simulations are compared with data for the indentation of a low alloy steel (EN24) substrate with a Young's modulus of 205 GPa, yield strength of 580 MPa and a Poisson's ratio of 0.3. The material was assumed to strain harden with the post-yield stress–strain behaviour given by the power law relation, (Eq. (5)). Analyses were carried out for the case of $n = 5$ and also for a perfectly plastic material ($n = \infty$). The comparison between the axisymmetric finite element simulations and the experimental Vickers indentation curve is shown in Fig. 4. It may be seen that an excellent agreement has been obtained between the finite element results for the 70° conical indenter with $n = 5$ and the measured Vicker's curve.

In spite of the inherent uncertainties as to the exact hardening behaviour of the substrate material, the close agreement for a typical value of $n = 5$ is encouraging and indicates that the results for the 70° conical indenter can in principle be used to analyse Vickers and, by extension, Berkovich indentation loading curves. Three-dimensional analyses of the indentation experiments are ongoing (COMPWERC, 1999) to further assess the validity of using axisymmetric assumptions to interpret the behaviour of Vickers and Berkovich indenters.

4.1. Comparison with the cavity model

The indentation curve predicted by the cavity model (Johnson, 1985) discussed earlier is also shown in Fig. 4. The very close agreement between the non-hardening finite element solution and the cavity model is evident. The slight discrepancy is believed to be due to the fact that in deriving the cavity model, it is

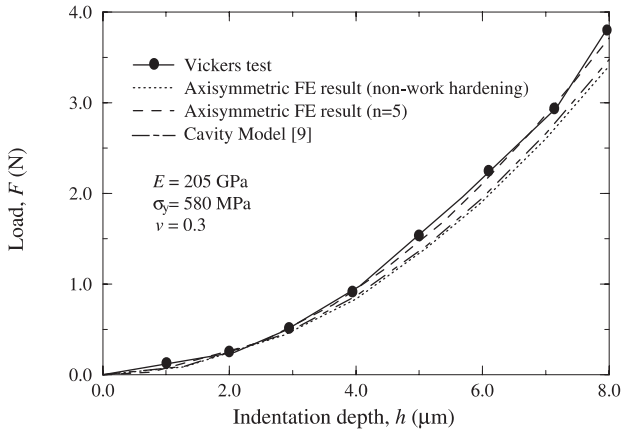

Fig. 4. An indentation curve for a low alloy steel.

assumed that no *piling-up* or *sinking-in* of material takes place around the indenter. However, in a real indentation test, due to the different material flow patterns in the contact region, piling-up or sinking-in can take place. This effect is fully accounted for in the large strain finite element formulation employed here. Similar conclusions were recently reached in the work of Cheng and Cheng (1999) where hardness predictions from the cavity model were compared with those obtained from the finite element simulations. It was found that the cavity model can overestimate or underestimate the hardness depending on whether sinking-in or piling-up occurs. A discussion of hardness measurements will be presented later in the text.

5. Parametric studies of the indentation of a coated system

We next examine the indentation of coated substrates and illustrate the use of the dimensionless scaling functions derived in Section 2 to extract coating material properties. All simulations of the coating/substrate systems were carried out to the same maximum indentation depth of 33% of the coating thickness, h_o. This choice of indentation depth minimises the possibility of yielding in the substrate and justifies the assumption of linear elastic behaviour in the substrate. Poisson's ratio was taken to be 0.3 for both the coating and substrate material in all simulations. Results are first presented for the case of an elastic, perfectly plastic coating ($n_c = \infty$) and then for a strain hardening coating material. The simulations were undertaken for a variety of coating materials characterised by a range of yield strengths and Young's moduli, (i.e. a range of σ_{yc}/E_s and E_c/E_s). For the latter, in the interest of space, comprehensive results are presented only for three typical Young's modulus ratios, $E_c/E_s = 0.1$, 1, and 10.

5.1. Indentation of an elastic, perfectly plastic coating

The function $\hat{\Pi}_\delta$ which relates the initial unloading slope to the coating mechanical properties is first examined.

Finite element results, showing the dependence of the dimensionless initial unloading slope in Eq. (10) on normalised yield strength (σ_{yc}/E_s), are presented in Fig. 5 for $E_c/E_s = 0.1$, 1, and 10. Since the simulations were carried out to the same maximum indentation depth of $h_m/h_o = 0.33$, all the unloading slopes correspond to the same normalised indentation depth.

Fig. 5 shows that, for the given values of v_c, v_s, h_m, and θ, the initial unloading slope of an elastic, perfectly plastic coating material is relatively insensitive to σ_{yc}/E_s, and is only a function of E_c/E_s. For an elastic, perfectly plastic coating material, this observation implies that

$$\left.\frac{1}{h_o E_s}\frac{dF}{dh}\right|_{h=h_m} = \hat{\Pi}_\delta\left(\frac{E_c}{E_s}\right), \tag{11}$$

with v_c, v_s, n_c, θ, and h_m fixed. An equivalent expression for an uncoated substrate was presented by Cheng and Cheng (1999), where the initial normalised unloading slope depended only on the substrate Young's modulus. In Fig. 6, a log–log plot of the normalised unloading slope versus Young's modulus ratio is provided. This curve allows an immediate identification of the Young's modulus of the coating from the initial unloading slope of the indentation curve, if the coating thickness (h_o) and the substrate Young's modulus (E_s) are known.

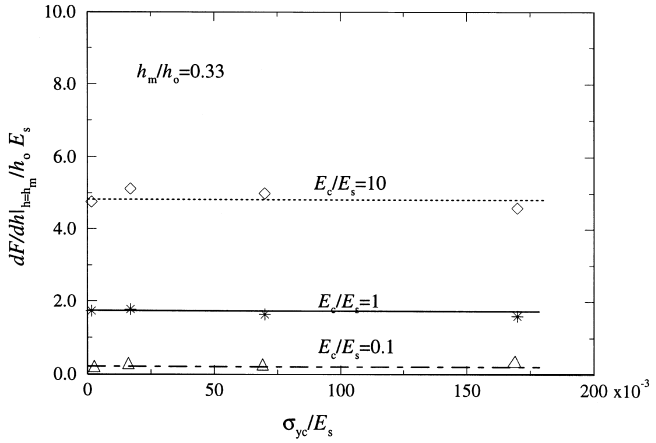

Fig. 5. Relationship between the initial unloading slope, and σ_{yc}/E_s.

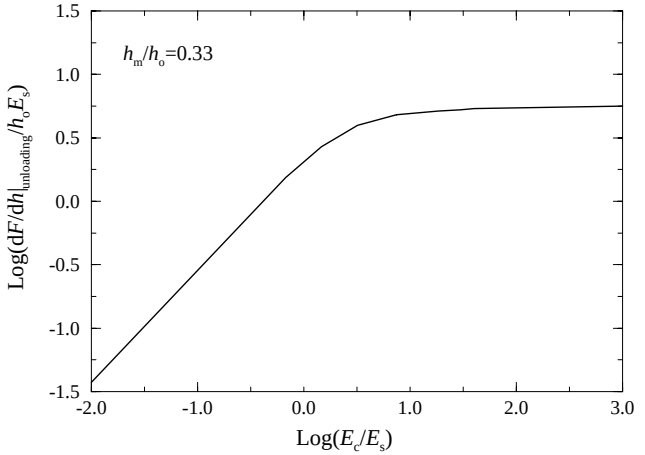

Fig. 6. Relationship between the initial unloading slope and E_c/E_s.

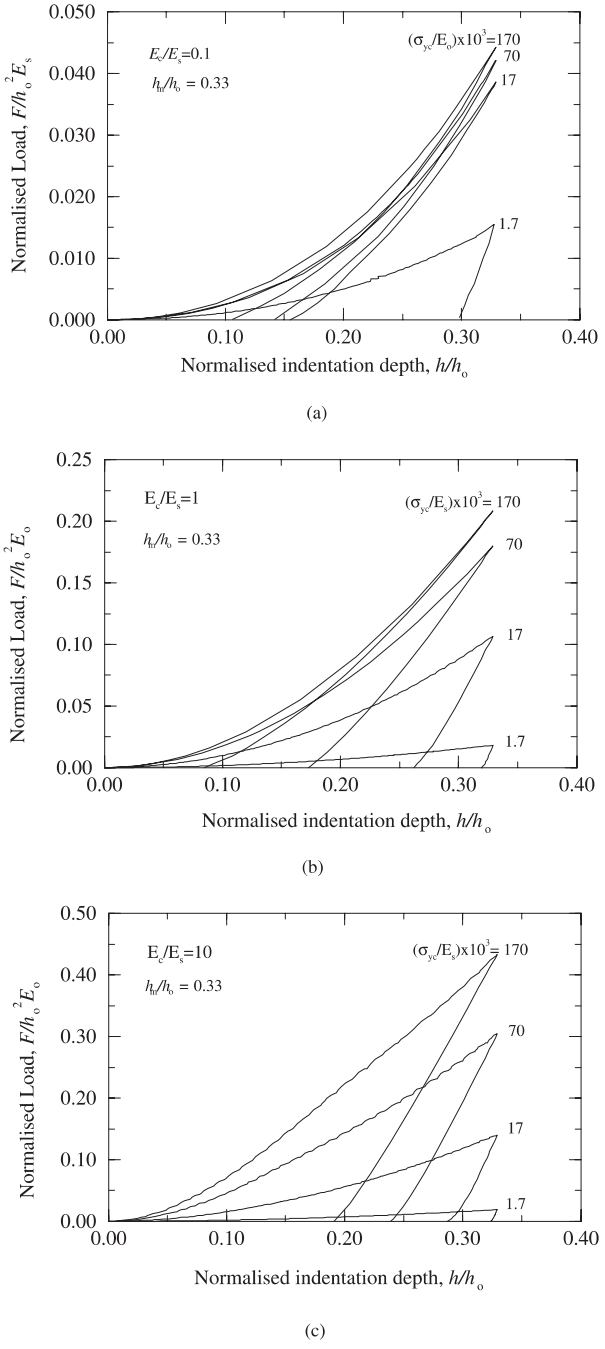

Fig. 7. Normalised indentation curves for a perfectly plastic coating: (a) $E_c/E_s = 0.1$, (b) $E_c/E_s = 1$, and (c) $E_c/E_s = 10$.

The dimensionless function, $\hat{\Pi}_\beta$ in Eq. (9), is next examined. Fig. 7(a)–(c) show the computed normalised indentation load, F/h_o^2E, vs. normalised displacement, h/h_o, for various σ_{yc}/E_s values with $E_c/E_s = 0.1$ in Fig. 7(a), $E_c/E_s = 1$ in Fig. 7(b), and $E_c/E_s = 10$ in Fig. 7(c). The systematic studies

conducted as a part of this work have shown that, for different values of h_o, the form of $\hat{\Pi}_\beta$ in Eq. (7) is retained, i.e. when the load–indentation curves are normalised as in Fig. 7, they collapse onto a single distribution. In Fig. 8, the normalised maximum indentation load ($F_{max}/h_o^2E_s$) from Fig. 7 as a function of the normalised coating yield strength (σ_{yc}/E_s), for $E_c/E_s = 0.1$, 1, and 10, is shown. The almost constant value of a normalised indentation load ($F_{max}/h_o^2E_s$) at highly normalised coating yield strength (σ_{yc}/E_s) for $E_c/E_s = 0.1$, in Fig. 8 is due to the relatively large scale used (see Fig. 7a where the difference in the normalised maximum load for the different values of a normalised yield stress is seen more clearly).

Using Figs. 6 and 7, the mechanical properties of the coating can be readily extracted from an indentation test with a 70° conical indenter or a Vickers or Berkovich indenter. Young's modulus of the coating material can first be estimated from the initial unloading slope using the curve given in Fig. 6. The coating yield strength, σ_{yc} can then be determined by normalising the experimental loading curve as in Fig. 7 and finding its best match among the numerically determined ones in Fig. 7, for the particular E_c/E_s ratio determined in the previous step. More directly, σ_{yc} can be determined from Fig. 8 by matching the normalised experimental maximum load at $h_m = 0.33h_o$ with the simulated one for the value of E_c/E_s obtained from Fig. 6. However, for the $E_c/E_s = 0.1$ case, a replotting of the curve presented in Fig. 8 on a more appropriate scale may be required.

The analyses presented here are for three selected values of E_c/E_s. Further studies on a wider range of E_c/E_s values are underway (COMPWERC, 1999).

5.2. Effect of strain-hardening on indentation curve

In this section, the effect of strain-hardening on the indentation response of the coated substrate is examined. The post-yield stress–strain behaviour of the coating is assumed to be described by the power law relation (Eq. (5)) and the functional relationships given in Eqs. (7) and (10) for a strain hardening coating material are next determined. Simulations were performed for a range of σ_{yc}/E_s ratios and three values of E_c/E_s. Materials with a moderate ($n_c = 10$) and strong ($n_c = 5$) hardening behaviour were considered. The results are presented in Figs. 9–15.

Fig. 9 examines the effect of strain-hardening on the initial unloading slope for the three Young's modulus ratios. It can be seen that the value of the initial unloading slope is nearly insensitive to the value

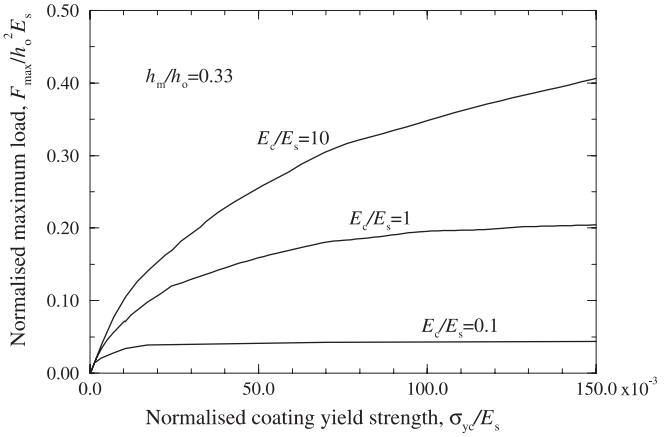

Fig. 8. Normalised maximum indentation load against the normalised coating yield strength.

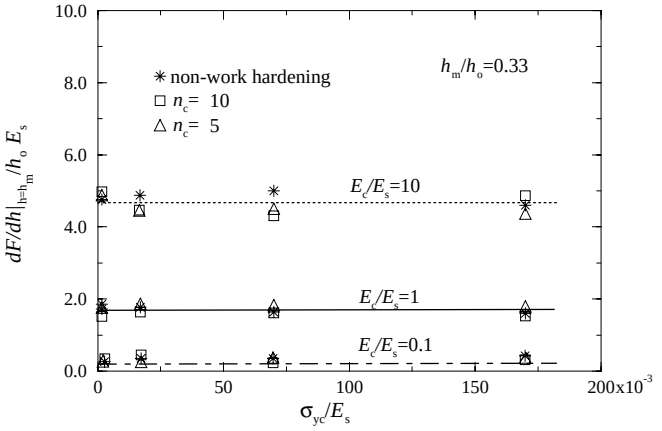

Fig. 9. Relationship between the initial unloading slope when $h_m/h_o = 0.33$, and σ_{yc}/E_s.

of a strain-hardening exponent, n_c. Hence, the relationship given in Eq. (11) also applies to a work-hardening coating material and Fig. 6 can then be used to estimate Young's modulus of a work-hardening coating material from the initial unloading slope measured in an indentation test. The error in assuming that the unloading slope is independent of n_c may be gauged from Figs. 6 and 9 and is estimated to be about 10% for $n = 10$ and $E_c/E_s = 10$.

Fig. 10 shows the normalised load vs. indentation depth curves for perfectly plastic and work-hardening coatings. Results are presented as before for three values of σ_{yc}/E_s and three values of E_c/E_s. It may be seen that for high values of σ_{yc}/E_s the work-hardening exponent has little effect on the indentation curve for $E_c/E_s = 0.1$ and $E_c/E_s = 1$. This observation can be explained by referring to Fig. 11, where the maximum plastic strain is plotted against σ_{yc}/E_s for $E_c/E_s = 1$. Here, the magnitude of the maximum accumulated plastic strain at large values of σ_{yc}/E_s, is significantly smaller than that at smaller σ_{yc}/E_s ratios. At this indentation depth, h_m/h_o, the elastic strain at high values of σ_{yc}/E_s is therefore sufficiently large to accommodate most of the deformation and the indentation curves depend only weakly on the material strain-hardening behaviour.

The normalised maximum load vs. coating yield strength for the different hardening exponents is plotted in Fig. 12. It is seen that, for $E_c/E_s = 0.1$ and 1 the normalised maximum load depends weakly on n_c particularly at large values of σ_{yc}/E_s (due to the reasons discussed above). It is also clear that for a given value of E_c/E_s a number of combinations of σ_{yc}/E_s and n_c can give the same maximum normalised indentation load. The implication of this is demonstrated by the result shown in Fig. 13. This figure shows the indentation curves for two materials with very different uniaxial behaviour – an elastic, perfectly plastic material with $\sigma_{yc}/E_s = 70$ and a strain-hardening material with $\sigma_{yc}/E_s = 40$ and $n_c = 5$ (both have $E_c/E_s = 10$). It can be seen that both materials produce almost identical indentation curves. This illustrates that the indentation curves alone cannot be used to determine yield strength and hardening behaviour for strongly work-hardening materials.

In order to differentiate the indentation responses of these two materials, we examine the local deformation in the contact region. Fig. 14 shows the contours of normalised stress plotted on the deformed configuration for the two cases addressed in Fig. 13. Both figures are plotted to the same scale. It may be seen that the two materials exhibit different stress distributions in the contact region – the hardening material (Fig. 14(a)) experiences higher stresses in the contact region than the non-hardening material (Fig. 14(b)). It may also be noted that the contact radius, r_c is different in each case even though the indentation depth is the same. The hardening material experiences sinking-in around the indenter (Fig. 14(a)) while the

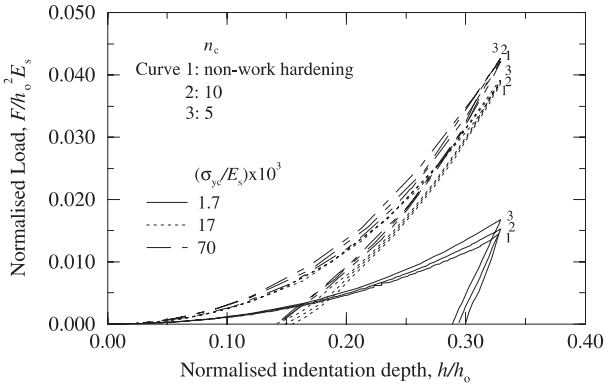

(a)

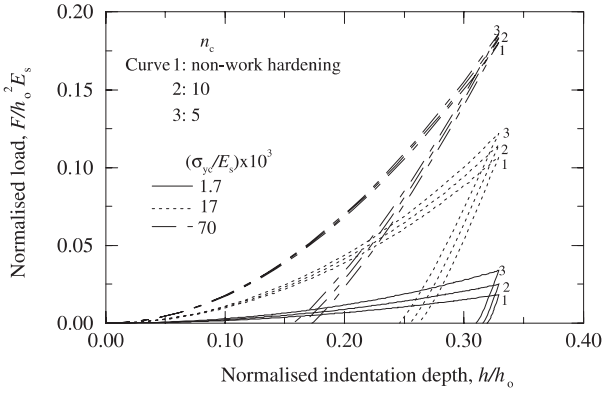

(b)

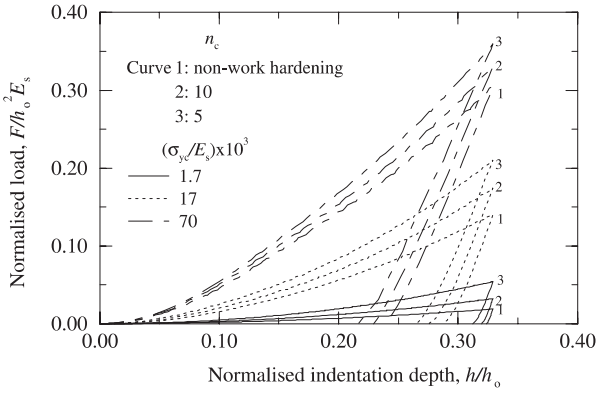

(c)

Fig. 10. Normalised indentation curves accounting for the material strain-hardening: (a) $E_c/E_s = 0.1$, (b) $E_c/E_s = 1$, and (c) $E_c/E_s = 10$.

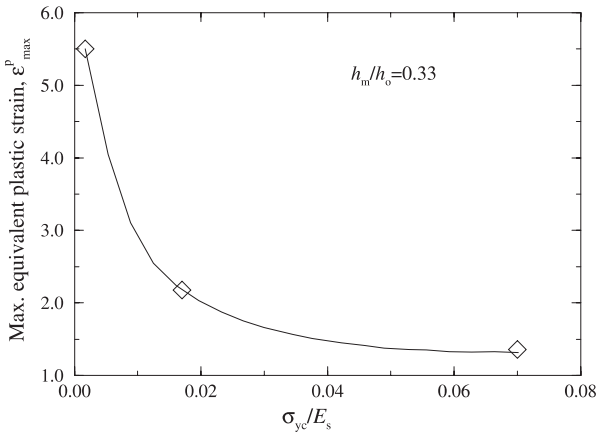

Fig. 11. The effect of coating dimensionless yield strength on the computed maximum equivalent plastic strain, ($E_c/E_s = 1$, $n_c = \infty$).

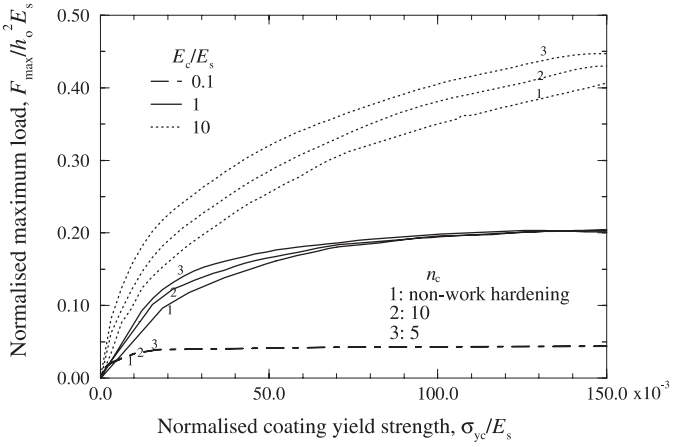

Fig. 12. Normalised maximum indentation load against the normalised coating yield strength for three values of strain-hardening.

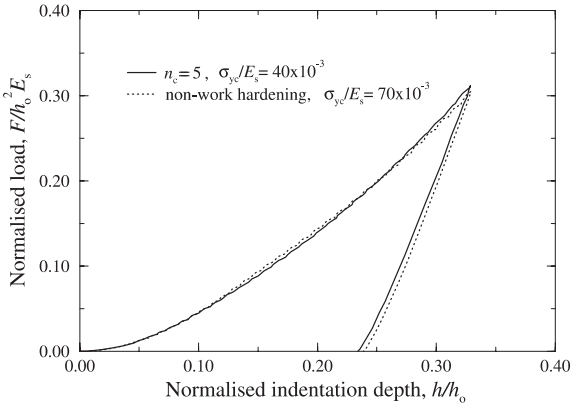

Fig. 13. Indentation curves for two materials with different uniaxial post-yield behaviour.

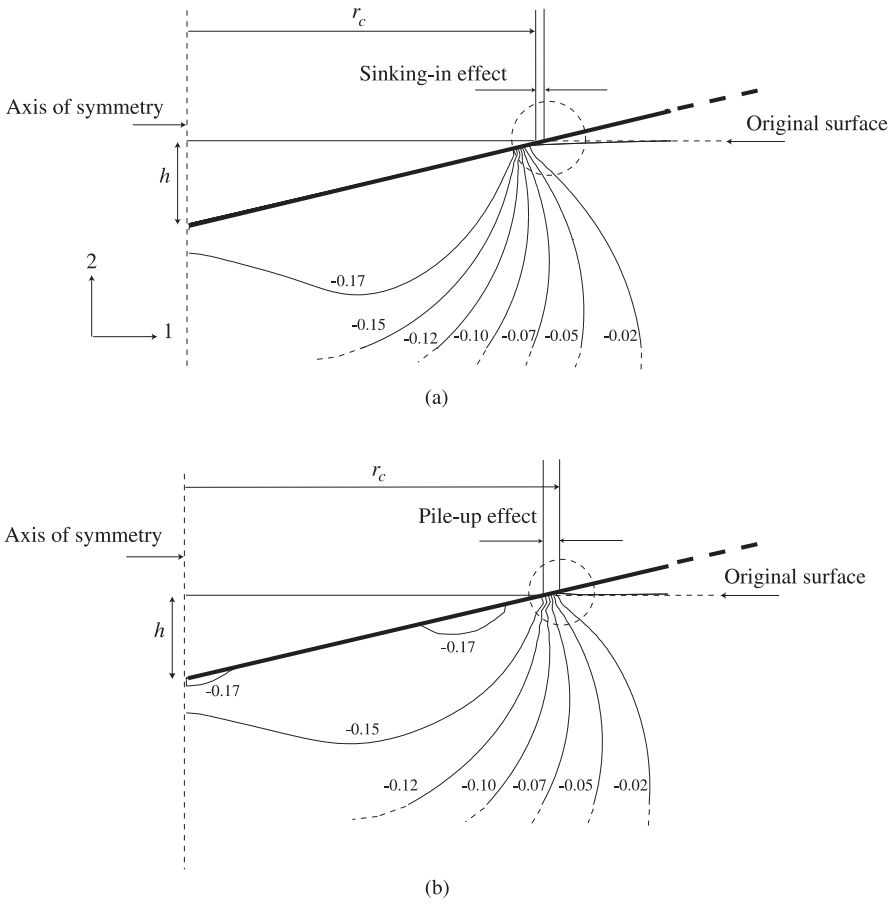

Fig. 14. Contour plot of the normalised stress (σ_{22}/E_s) in the contact region at the same indentation depth h: (a) $n_c = 5$, $\sigma_{yc}/E_s = 40 \times 10^{-3}$ (b) elastic–perfectly plastic, $\sigma_{yc}/E_s = 70 \times 10^{-3}$.

non-hardening material experiences pile-up (Fig. 14(b)) resulting in a higher contact area in the latter case. In the absence of pile-up or sinking-in, the contact radii at the same indentation depth must be the same. Thus, these two materials which have the same normalised indentation force have different stress distributions in the contact area and different associated contact radii.

To extract unique values of n_c and σ_{yc} from an indentation test, a two-step approach is proposed based on an additional matching parameter, here chosen as the final value of the contact area after unloading, denoted by A_f. In this work, A_f is calculated by

$$A_f = \pi(r_{cf})^2, \tag{12}$$

where r_{cf} is the corresponding contact radius defined as the radial distance from the axis of symmetry to the point of last contact (Pethica et al., 1983; Oliver et al., 1986). (Note that A_f and r_{cf} depend on the value of h_m.) Fig. 15 displays the relationship between the normalised final area of contact (A_f/h_o^2) and coating yield strength for different strain hardening exponents and three E_c/E_s ratios.

Fig. 12 in combination with Fig. 15 can then be used to evaluate the yield strength and strain-hardening properties of the coating material after the coating, Young's modulus has been determined. For a known value of F_{max}, a range of possible values for the coating yield strength and the corresponding

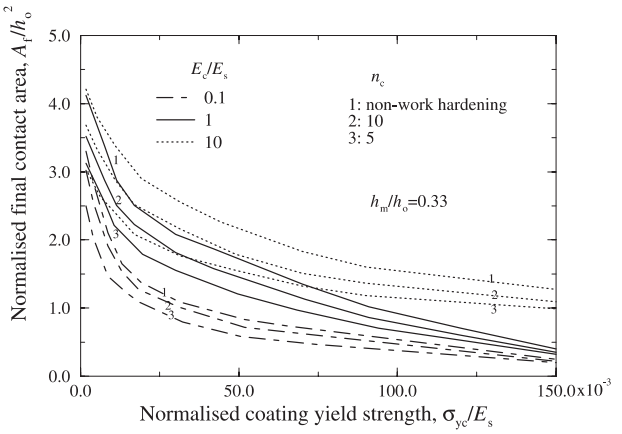

Fig. 15. Normalised final contact area against the normalised coating yield strength.

strain-hardening exponent can be obtained from Fig. 12. Fig. 15 can subsequently be used to select the correct pair of yield strength and hardening exponent among those pre-predicted by Fig. 12. For example, consider the case which yielded values of $E_c/E_s = 10$, $F_{max}/h_o^2E_s = 0.3$ and $A_f/h_o^2 = 1.92$. Fig. 12 gives the following possible ratios of a normalised yield stress: $\sigma_{yc}/E_s \approx 42$, 55 and 68 $\times 10^{-3}$ for $n_c = 5$, 10 and ∞, respectively. Fig. 15 gives three other possible values of σ_{yc}/E_s, i.e ≈ 24, 43 and 68 $\times 10^{-3}$ for $n_c = 5, 10$ and ∞ respectively. It may be deduced therefore that the value of the yield strength and the hardening exponent estimated from this approach are $68 \times 10^{-3}E_s$ and ∞, respectively.

It may be noted that the lower curve ($E_c/E_s = 0.1$) in Fig. 12 shows almost no sensitivity to the value of n_c. However, the contact area curves in Fig. 15 for this value of $E_c/E_s = 0.1$ does show a dependence on n_c. Thus, the approach can obtain values for σ_{yc} and n_c for this E_c/E_s ratio. As discussed earlier, a smaller scale for Fig. 12, is more appropriate at lower values of E_c/E_s.

6. Hardness estimation using the finite element method

Hardness is generally defined as the mean pressure supported by the material under load (Pharr et al., 1995),

$$H = \frac{F_{max}}{A}, \tag{13}$$

where F_{max} is the maximum load and A is the projected area of contact under load. Generally, A cannot be determined directly, but must be inferred from the final indentation area after the load has been removed.

In this section, a method to estimate the measure of hardness (H) defined in Eq. (13) is proposed. Numerically determined values of A have been obtained and are plotted against the coating yield strength for $E_c/E_s = 10$ in Fig. 16. Once the material properties of the coating, i.e E_c/E_s, σ_{yc}/E_s, and n_c, have been obtained using the approach discussed in the previous section, the value of A can then be determined directly from Fig. 16. Subsequently, the hardness H, can be calculated from Eq. (13).

In the conventional (Meyer) method of calculating hardness, A is estimated from an optical observation of the residual projected area of the impression after unloading (Tabor, 1951), i.e., A_f in this work. By comparing Figs. 15 and 16, it may be observed that this method can overestimate the contact area (by up to 66%) at high value of coating yield strength where a significant portion of the contact area at maximum

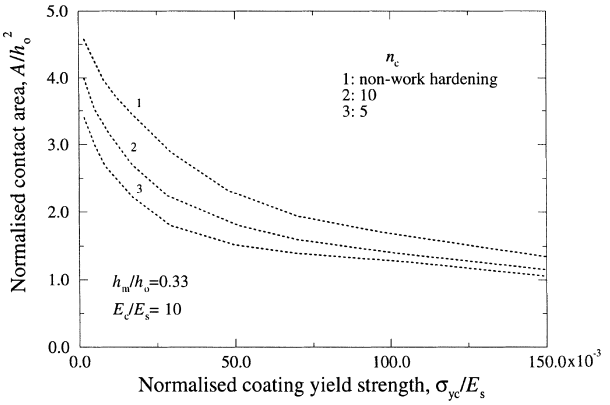

Fig. 16. Normalised contact area at maximum load ($h_m/h_o = 0.33$) against the normalised coating yield strength.

depth is due to an elastic deformation. Consequently, the residual projected area after unloading is smaller than the projected contact area at maximum penetration, and the conventional hardness method can considerably overestimate the contact area (Gubicza et al., 1996).

Recently, a method to estimate A was developed by Oliver and Pharr (1992) in which the contact area can be determined from the indentation curve without the need for optical measurements. The area of contact under load can be estimated from the following:

$$A_{O/P} = \pi(h_m - \alpha F_{max}/S)^2 \tan^2\theta, \tag{14}$$

where, α is the indenter shape parameter (=0.75 for a conical indenter), and S, the initial unloading slope ($= dF/dh|_{h=h_m}$). The values of the contact area obtained from the Oliver and Pharr method, $A_{O/P}$, normalised by the numerically determined contact area at maximum depth (for $E_c/E_s = 1$) are plotted against the coating yield strength in Fig. 17. It may be seen that the O/P method underestimates the value of contact area at low values of coating yield strength by up to 40%, and overestimates it by up to 20 % for high values of σ_{yc}/E_s. Some error in the O/P method is expected since it does not account for the mismatch in material properties between the coating and the substrate. The relatively poor agreement at low values of σ_{yc}/E_s is

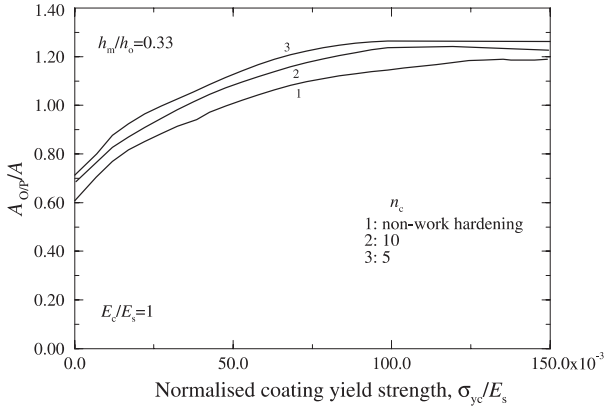

Fig. 17. Normalised contact area calculated by the Oliver and Pharr (1992) method against normalised coating yield strength ($E_c/E_s = 1$, $h_m/h_o = 0.33$).

due to the fact that, while the O/P method includes the effects of sinking-in of the material, it does not account for the significant amount of pile-up encountered with low yield strength coatings. The pile-up in the latter case is also exacerbated by the constraint imposed on the plastic deformation in the coating by the relatively non-deformable substrate. The O/P method therefore considerably underestimates the area under load for low strength coatings, $\sigma_{yc}/E_s < 25 \times 10^{-3}$. Similar observations have been made by Pharr et al. (1995) where hardness predictions from the O/P method for thin films were compared with those obtained directly from the finite element simulations and also by Cheng and Cheng (1998a,b) where the applicability of the O/P method to determine contact depth for uncoated substrates from indentation curves were discussed. Eq. (14) therefore provides a rather approximate estimate of the contact area required in the definition of an appropriate coating hardness measure.

7. Discussion and conclusions

A method for determining the elastic–plastic properties of the coating materials from an indentation test has been introduced, which combines dimensional analysis and finite element simulations. Appropriate scaling functions to describe the indentation process have been developed and the finite element simulations performed for a variety of coating systems characterised by Young's modulus, yield strength, and work-hardening exponent. While the simulations have been carried out for a conical indenter, the indenter angle was chosen so that the results presented here can also be used to extract the mechanical properties of a coating material from indentation curves produced with Vickers or Berkovich-type indenters.

The results show that, for the given values of coating and substrate Poisson's ratio, and indenter geometry, the initial unloading slope of the indentation curve is a function of the ratio of coating and substrate Young's modulus only. Therefore, Young's modulus can be extracted from an indentation unloading curve provided that the Young's modulus of the substrate is known. The yield strength, for a perfectly plastic or low-hardening coating, can then be evaluated by matching the maximum load measured experimentally with the simulated ones for that particular ratio of coating and substrate moduli. The yield strength for a strongly work-hardening material, on the other hand, cannot be directly estimated using the same method since the effect of the hardening exponent and that of the yield strength cannot be separately identified from the maximum indentation load. However, it has been shown that by introducing curves of a normalised final contact area against normalised yield strength, the value of coating yield strength and hardening exponent can be uniquely determined. Once the coating material properties have been determined, the value of the contact area under load which is required for an accurate estimation of the coating hardness can be obtained directly from curves such as those presented in Fig. 16. The proposed method could easily be extended to include an additional dependence of the functional relationships on, for example, the substrate yield strength, σ_{ys}, which will introduce additional dimensionless variables into Eq. (7) (e.g., σ_{yc}/σ_{ys}, E_c/σ_{ys}, etc.).

A relatively simple description of the coating material behaviour has been assumed in the analysis – Von Mises flow theory with perfectly plastic or power law hardening material behaviour. Depending on the relevant material length scales, i.e. coating thickness/grain size, indenter radius of curvature/grain size, a continuum isotropic description of the material response may not be representative of the true local behaviour. Furthermore, residual stress effects, which may be significant for certain coating-substrate systems, have also been neglected in the analysis. In practice, the relevance of the results presented here may be gauged from the experimental curves. If the shape of the indentation curves differ significantly from those presented here, or the proposed scaling laws do not apply, this would suggest that the material description used in this work is inadequate. It is expected that the results of this work, particularly those related to the coating yield strength and strain hardening exponent, will be most applicable for coating dimensions on the order of 100 μm evaluated by micro-indentation tests, and may not be practical for the very small size scales

associated with nano-indentation since accurate measurement of the final contact area may be very difficult to obtain. Also, the influence of the sharp edges and flat contact faces of the Berkovich type indenter on the indentation curve, which may be important in nano-indentation, is not accounted for here. At present, the approach described in this work is being evaluated in connection with micro-indentation of Mo coatings (of 100 μm thickness) on steel substrates (COMPWERC, 1999).

Acknowledgements

Support for this work was provided by the government of Thailand. Helpful discussions with the COMPWERC group (Brite EUram project, BE97-4283), in particular Dr.P.E. McHugh and Mr.L. Farrissey of NUI, Galway are gratefully acknowledged. Dr. O'Dowd acknowledges useful discussions with Dr. Seán Leen of Nottingham University. The indentation tests were carried out at the Department of Mechanical Engineering, Imperial College, UK, as a part of the final year project of Mr. C. Nou. ABAQUS was provided under academic license by HKS Inc., Providence, RI, USA.

References

ABAQUS version 5.7, Hibbitt, Karlsson and Sorensen, Providence, RI.

Barenblatt, G.I., 1996. Scaling, self-similarity, and intermediate asymptotics. Cambridge University Press, London.

Bhattacharya, A.K., Nix, W.D., 1988. Finite-element, simulation of indentation experiments. Int. J. Solids Struct. 24 (9), 881.

Bolshakov, A., Pharr, G.M., 1998. Influences of pileup on the measurement of mechanical properties by load and depth sensing indentation techniques. J. Mater. Res. 13 (4), 1049.

Cheng, Y.T., Cheng, C.M., 1998a. Scaling approach to conical indentation in elastic–plastic solids with work hardening. J. Appl. Phys. 84 (3), 1284.

Cheng, Y.T., Cheng, C.M., 1998b. Further analysis of indentation loading curves: effects of tip rounding on mechanical property measurements. J. Mater. Res. 13 (4), 1059.

Cheng, Y.T., Cheng, C.M., 1998c. Effect, of 'sinking in' and 'piling up' on estimating the contact area under load in indentation. Phil. Mag. Lett. 78 (2), 115.

Cheng, Y.T., Cheng, C.M., 1999. Scaling relationships in conical indentation of elastic–perfectly plastic solids. Int. J. Solids Struct. 36, 1231.

COMPWERC, 1999, Brite EuRam project, BE97-4283.

Doerner, M.F., Nix, W.D., 1986. J. Mat. Res. 1, 601.

Gubicza, J., Juhasz, A., Lendvai, J., 1996. A new method for hardness determination from depth sensing indentation tests. J. Mater. Res. 11 (12), 2964.

Johnson, K.L., 1985. Contact Mechanics. Cambridge University Press, London.

Knapp, J.A., Follstaedt, D.M., Myers, S.M., Barbour, J.C., Friedmann, T.A., 1999. Finite-element modeling of nanoindentation. J. Appl. Phys. 85 (3), 1460.

Laursen, T.A., Simo, J.C., 1992. A study of the mechanics of microindentation using finite-elements. J. Mat. Res. 7 (3), 618.

Oliver, W.C., Hutchings, R., Pethica, J.B., 1986. ASTM STP 889, 90.

Oliver, W.C., Pharr, G.M., 1992. An improved technique for determining hardness and elastic modulus using load and displacement sensing indentation experiments. J. Mat. Res. 7, 1564.

Pethica, J.B., Hutchings, R., Oliver, W.C., 1983. Hardness measurement at penetration depths as small as 20 nm. Philo. Mag. A 48, 593.

Pharr, G.M., Bolshakov, A., Tsui, T.Y., Hay, J.C., 1995. Nonoindentation of soft films on hard substrates: experiments and finite element simulations. J. Mat. Res., in press.

Sneddon, I.N., 1965. Int. J. Engng. Sci. 3, 47.

Tabor, D., 1951. Hardness of Metals. Clarendon Press, Oxford.

Vlassak, J., Tsui, T.Y., Nix, W.D., 1999a. Indentation plastic displacement field: part I, the case of soft films on hard substrates. J. Mat. Res. 14 (6), 2196.

Vlassak, J., Tsui, T.Y., Nix, W.D., 1999b. Indentation plastic displacement field: part II, the case of hard films on soft substrates. J. Mat. Res. 14 (6), 2204.